

# Onset of Convection in a Porous Layer with Continuous Periodic Horizontal Stratification. Part I. Two-Dimensional Convection

D. Andrew S. Rees · Peder A. Tyvand

Received: 22 October 2008 / Accepted: 12 December 2008 / Published online: 24 January 2009  
© Springer Science+Business Media B.V. 2009

**Abstract** The onset of convection in a horizontal porous layer is investigated theoretically. The permeability of the porous medium is a continuous periodic function of the horizontal  $x$  coordinate. Floquet theory has been employed to determine the favoured two-dimensional mode of convection. For a wide range of periods of the permeability variation, a matrix eigenvalue technique with eighth order accuracy has been employed to find the critical Darcy–Rayleigh number. This is supplemented by a multiple-scales analysis of the large-period limit, and a brief consideration of the anisotropic limit for very short periods.

**Keywords** Free convection · Nonuniform permeability · Linear stability theory · Floquet theory · Multiple scales theory

## Nomenclature

$a$	Central difference coefficients for a first derivative
$b$	Central difference coefficients for a second derivative
$f, g$	Reduced forms of the perturbations
$\underline{f}, \underline{g}$	Vector forms of the perturbations
$F$	Nondimensional permeability variation
$H$	Height of the porous layer
$k$	Wave number of the permeability variations
$K$	Permeability
$K_0$	Mean permeability
$M_1$ – $M_4$	Matrices used in the numerical method

---

D. A. S. Rees (✉)  
Department of Mechanical Engineering, University of Bath, Bath BA2 7AY, UK  
e-mail: ensdars@bath.ac.uk

P. A. Tyvand  
Department of Mathematical Sciences and Technology, Norwegian University of Life Sciences,  
P.O. Box 5003, 1432 Ås, Norway

$N$	Number of intervals in the numerical scheme
$p$	Pressure
$P$	Period of the permeability variation
$R_0, R_1, R_2$	Terms in the small- $k$ expansion for Ra
Ra	Darcy–Rayleigh number
$T$	Temperature
$T_c, T_h$	Cold and hot boundary temperatures, respectively
$x$	Horizontal coordinate
$y$	Horizontal (spanwise) coordinate
$z$	Vertical coordinate
$u$	Horizontal velocity
$v$	Horizontal (spanwise) velocity
$w$	Vertical velocity

### Greek letters

$\beta$	Coefficient of thermal expansion
$\epsilon$	Relative amplitude of the permeability variation
$\theta$	Nondimensional temperature
$\kappa_m$	Thermal diffusivity of the porous medium
$\mu$	Dynamic viscosity
$\nu$	Floquet exponent
$\xi$	Anisotropy parameter
$\hat{\chi}$	Scaled form of $\chi$
$\rho_0$	Reference density
$\rho$	Density
$\sigma$	Heat capacity ratio of the porous medium to that of the fluid
$\chi$	Slow $x$ -variable
$\psi$	Streamfunction
$\omega$	Scaled Floquet exponent

### Subscripts and superscripts

$c$	Critical conditions
$i, j$	Denoting grid points
$0,1,2$	Terms in the small- $k$ expansion
$\chi$	Partial derivatives with respect to $\chi$
$\bar{\phantom{x}}$	Dimensional variables
$\hat{\phantom{x}}$	Reduced variables
$\prime$	Derivative with respect to $x$

## 1 Introduction

The problem of convection instability in a porous medium heated from below was first solved by Horton and Rogers (1945) and later by Lapwood (1948), Wooding (1957) and Beck (1972). These pioneering articles assumed a homogeneous and isotropic porous medium. The first study of convection in an inhomogeneous porous medium was performed by

Gheorghitza (1961). Rana et al. (1979) investigated convection in multi-layered geothermal reservoirs. McKibbin and O'Sullivan (1980, 1981) solved the problems of onset of convection and weakly nonlinear convection with discrete horizontal sublayers. Rees and Riley (1990) extended the analysis of McKibbin and O'Sullivan by determining regions in parameter space where the expected pattern of convection is three-dimensional. McKibbin and Tyvand (1982), McKibbin and Tyvand (1983), McKibbin and Tyvand (1984) investigated the convergence to homogenous anisotropy for convection cells that penetrate multiple horizontal porous layers with alternating permeabilities or thermal conductivities. Gjerde and Tyvand (1984) solved the related problem of onset of convection with the permeability given as a continuous periodic function of the vertical coordinate.

The onset of convection in anisotropic porous media had earlier been investigated by Castinel and Combarous (1974), Epherre (1975) and Wooding (1978). This was extended to supercritical nonlinear convection by Kvernfold and Tyvand (1979).

The above-mentioned articles on inhomogeneous media concentrated on Darcy–Bénard (or Horton–Rogers–Lapwood) convection with horizontal layers, which means that variations in the permeability and/or conductivity occur only in the vertical direction. The onset of convection and the problem of slightly supercritical convection have been studied, and the solutions have been compared with an average description in terms of uniform anisotropy.

In the literature, the presence of vertical layers has been considered less often than when the layers are horizontal. The onset of Rayleigh–Bénard convection in a porous cavity containing vertical layers was investigated by McKibbin (1986). He also carried the analysis into the nonlinear domain of steady supercritical convection. However, his analysis was restricted to two-dimensional flow in a finite cavity. It is physically plausible that the preferred mode of convection will be three-dimensional if the vertically-layered porous medium is of infinite horizontal extent. Even if convection is restricted to two dimensions, then the periodicity of the onset mode is unlikely to be the same as that of the property variations. Thus this study continues the two-dimensional linearised analysis by McKibbin (1986), but with two modifications. We assume vertical layering in terms of continuous (as opposed to a discrete) periodic stratification in the  $x$ -direction. We also let the porous medium be unbounded in the horizontal  $x$ -direction. We will solve numerically the linearised two-dimensional onset problem. We will give a separate analysis of the long-wavelength limit as well as the short-wavelength limit of permeability variation. The latter limit is the limit of homogeneous anisotropy.

This study gives a theoretical investigation of the onset of Darcy–Bénard convection. There are a number of other studies on convection in layered porous media. For example, Reda (1986) published experiments on convection in layered porous media, and Poulikakos and Bejan (1983) investigated convection in a porous cavity heated from the side, by taking into account both horizontal and vertical layering. More references can be found in the review of Rees (2000), the book by Nield and Bejan (2006) and the article in the present issue by Nield et al. (2009).

## 2 Problem Formulation

We consider a porous layer of constant thickness  $H$ , saturated with viscous fluid with density  $\rho$  and dynamic viscosity  $\mu$ . The reference density is  $\rho_0$  and the coefficient of thermal expansion is  $\beta$ . We will consider periodic and continuous stratification in the  $x$ -direction where the permeability of the isotropic porous medium is  $K(\bar{x})$ , where  $K_0$  is the reference permeability and the spatial period of the variations is  $\bar{P}$ . The gravitational acceleration is  $g$ . The effective thermal diffusivity of the saturated porous medium is  $\kappa_m$ ; we treat this value

as a constant in this article although it will, in general, also vary with  $\bar{x}$ . We note that the diffusivity may either increase or decrease with increasing permeability depending on the relative diffusivities of the solid and fluid phases.

We assume that Darcy’s law and the Boussinesq approximation are valid, and that the fluid and the solid phases are in local thermal equilibrium. Subject to these constraints, the governing equations are,

$$\begin{aligned} \frac{\partial \bar{u}}{\partial \bar{x}} + \frac{\partial \bar{v}}{\partial \bar{y}} + \frac{\partial \bar{w}}{\partial \bar{z}} &= 0, & (1) \\ \bar{u} &= -\frac{K}{\mu} \frac{\partial \bar{p}}{\partial \bar{x}}, \quad \bar{v} = -\frac{K}{\mu} \frac{\partial \bar{p}}{\partial \bar{y}}, \quad \bar{w} = -\frac{K}{\mu} \left[ \frac{\partial \bar{p}}{\partial \bar{z}} - \rho g \beta (T - T_\infty) \right], & (2) \\ \kappa_m \left[ \frac{\partial^2 T}{\partial \bar{x}^2} + \frac{\partial^2 T}{\partial \bar{y}^2} + \frac{\partial^2 T}{\partial \bar{z}^2} \right] &= \bar{u} \frac{\partial T}{\partial \bar{x}} + \bar{v} \frac{\partial T}{\partial \bar{y}} + \bar{w} \frac{\partial T}{\partial \bar{z}} + \sigma \frac{\partial T}{\partial \bar{t}}, & (3) \end{aligned}$$

where all the terms are as defined in the Nomenclature. The boundary conditions are

$$\bar{z} = 0 : \quad \bar{w} = 0, \quad T = T_h, \quad \bar{z} = H : \quad \bar{w} = 0, \quad T = T_c. \tag{4}$$

These equations may be nondimensionalised upon introduction of the following substitutions,

$$(\bar{x}, \bar{y}, \bar{z}) = H(x, y, z), \quad (\bar{u}, \bar{v}, \bar{w}) = \frac{\kappa_m}{H}(u, v, w), \quad \bar{p} = \frac{\mu \kappa_m}{K_0} p, \quad T = T_c + (T_h - T_c)\theta, \quad \bar{t} = \frac{\sigma H^2}{\kappa_m} t. \tag{5}$$

Hence the governing Eqs. 1–3, become,

$$\begin{aligned} \frac{\partial u}{\partial x} + \frac{\partial v}{\partial y} + \frac{\partial w}{\partial z} &= 0, & (6) \\ u &= -F(x) \frac{\partial p}{\partial x}, \quad v = -F(x) \frac{\partial p}{\partial y}, \quad w = -F(x) \left[ \frac{\partial p}{\partial z} - \text{Ra} \theta \right], & (7) \\ \frac{\partial^2 \theta}{\partial x^2} + \frac{\partial^2 \theta}{\partial y^2} + \frac{\partial^2 \theta}{\partial z^2} &= u \frac{\partial \theta}{\partial x} + v \frac{\partial \theta}{\partial y} + w \frac{\partial \theta}{\partial z} + \frac{\partial \theta}{\partial t}, & (8) \end{aligned}$$

where the Darcy–Rayleigh number is defined as,

$$\text{Ra} = \frac{\rho_0 g \beta K_0 H (T_h - T_c)}{\kappa_m \mu}, \tag{9}$$

and where the function,  $F(x)$ , is a dimensionless permeability given by  $F = K(x)/K_0$ . We shall allow  $K$  to exhibit sinusoidal variations about its mean value, and therefore we set

$$F(x) = 1 + \epsilon \cos kx, \tag{10}$$

where  $\epsilon$  is the amplitude of the permeability variation which must satisfy  $0 \leq \epsilon < 1$ . The wavenumber,  $k$ , of the variation is related to its period via  $P = 2\pi/k$ , where  $P = \bar{P}/H$ .

In this article, we concentrate solely on two dimensional convection, such as would occur within a porous layer with a small spanwise dimension, or within an appropriately set up Hele Shaw cell. It is our intention to extend this analysis to three dimensions elsewhere. Therefore, we may set  $v = 0$  and define a streamfunction,  $\psi$ , in the usual way,

$$u = -\frac{\partial \psi}{\partial z}, \quad w = \frac{\partial \psi}{\partial x}, \tag{11}$$

Equations 6–8 reduce to the following system,

$$\frac{\partial^2 \psi}{\partial x^2} + \frac{\partial^2 \psi}{\partial z^2} - \frac{F'}{F} \frac{\partial \psi}{\partial x} = \text{Ra } F \frac{\partial \theta}{\partial x}, \tag{12}$$

$$\frac{\partial^2 \theta}{\partial x^2} + \frac{\partial^2 \theta}{\partial z^2} = \frac{\partial \psi}{\partial x} \frac{\partial \theta}{\partial z} - \frac{\partial \psi}{\partial z} \frac{\partial \theta}{\partial x}. \tag{13}$$

Given that the basic state whose stability we are addressing is given by  $\psi = 0$  and  $\theta = 1 - z$ , the linearised stability equations for perturbations to the basic state are given by (12) and

$$\frac{\partial^2 \theta}{\partial x^2} + \frac{\partial^2 \theta}{\partial z^2} = -\frac{\partial \psi}{\partial x} + \frac{\partial \theta}{\partial t}, \tag{14}$$

where  $\psi$  and  $\theta$  represent small-amplitude perturbations in the remainder of this article. The boundary conditions required to complete the statement of the linearised system are that,

$$\psi = \theta = 0 \quad \text{on} \quad z = 0, 1. \tag{15}$$

### 3 Floquet Analysis

The boundary conditions presented in Eq. 15 and the form of the perturbations equations, Eqs. 12 and 14, suggest that it is valid to factor out the function  $\sin \pi z$  from  $\psi$  and  $\theta$ . Such a technique has been used in previous articles by Rees and Lage (1997) and Rees and Tyvand (2004a,b) to great advantage. Therefore, we shall introduce the substitution:

$$(\psi, \theta) = (\hat{\psi}(x), \hat{\theta}(x)) e^{\lambda t} \sin \pi z, \tag{16}$$

where  $\lambda$  is the complex exponential growth rate for disturbances. The resulting equations are now,

$$\hat{\psi}'' - \pi^2 \hat{\psi} - \frac{F'}{F} \hat{\psi}' = \text{Ra } F \hat{\theta}', \tag{17}$$

$$\hat{\theta}'' - \pi^2 \hat{\theta} + \hat{\psi}' = \lambda \hat{\theta}, \tag{18}$$

where primes denote ordinary derivatives with respect to  $x$ .

It is now quite straightforward to prove that this system is subject to the principle of exchange of instabilities, i.e. that  $\text{Real}(\lambda) = 0$  also corresponds to  $\text{Imag}(\lambda) = 0$ . If we treat all the variables in Eqs. 17 and 18 as being complex, then we may multiply Eq. 17 by the complex conjugate of  $\hat{\psi}/F$ , multiply Eq. 18 by the complex conjugate of  $\text{Ra } \hat{\theta}$ , integrate both with respect to  $z$  in the range  $0 \leq z \leq 1$ , and subtract to obtain the expression,

$$\lambda \int_0^1 |\hat{\theta}|^2 dz = \int_0^1 \left[ \frac{1}{\text{Ra } F} (|\hat{\psi}'|^2 + \pi^2 |\hat{\psi}|^2) - (|\hat{\theta}'|^2 + \pi^2 |\hat{\theta}|^2) \right] dz. \tag{19}$$

It is clear that all of the integrals are real quantities, and therefore  $\lambda$  is always real. In the remainder of this article  $\lambda = 0$  is taken to be the condition for the onset of convection.

This configuration forms a mathematical problem with competing frequencies. The function,  $F$ , has frequency,  $k$ , and period,  $P$ , while the critical mode of convection in the absence of permeability variations has frequency (wavenumber),  $\pi$ , and a period equal to 2. As our intention is to examine the effect of permeability variation over a wide range of periodicities,

it is natural to adopt a Floquet analysis of the linearised equations. Therefore we may seek solutions of the form,

$$(\hat{\psi}, \hat{\theta}) = e^{i\nu kx/2} (f(x), g(x)) + \text{c.c.}, \quad (20)$$

where both  $f(x)$  and  $g(x)$  have period,  $P$ , and where c.c. denotes complex conjugate. However, the presentation of the equations is simplified if  $\nu$  is replaced by  $\omega$ , where  $\omega = \nu k/2$ . The functions  $f$  and  $g$  satisfy the complex equations,

$$f'' + 2i\omega f' - (\omega^2 + \pi^2)f - \frac{F'}{F}(f' + i\omega f) = \text{Ra} F(g' + i\omega g), \quad (21)$$

$$g'' + 2i\omega g' - (\omega^2 + \pi^2)g + (f' + i\omega f) = 0, \quad (22)$$

where the solutions need to be periodic with period,  $P$ . These equations form an eigenvalue problem for Ra as a function of  $P$  and  $\omega$ . While it is quite possible to effect their solution using a simple shooting method code with a high accuracy solver, such as a fourth order Runge Kutta scheme, we have chosen to adopt a matrix eigenvalue approach. Details of this method are given in Appendix A, but it is sufficient to say that we have taken an eighth-order accurate method, and our results are correct to at least six significant figures.

## 4 Numerical Results

### 4.1 Cellular Patterns

We begin our discussion of the numerical results by illustrating some of the flow patterns and how they vary with the value of the Floquet exponent,  $\nu$ , the permeability amplitude,  $\epsilon$ , and the period,  $P$ .

Figure 1 depicts the case  $P = 2$  (which corresponds to the critical wavelength for Darcy–Bénard convection in a uniform layer) with  $\epsilon = 0.3$ . A greyscale indication is also given in the figure to help illustrate clearly how the flow pattern is affected by the locations of regions of relatively high or low permeability. The case  $\nu = 0$  simply allows the onset mode to have the same periodicity as the background permeability variation. In this case, the flow is quite naturally stronger in those regions where the permeability is the highest, as evidenced by the concentration of streamlines there. It is also interesting to see that the stronger cells are slightly narrower than the weaker cells. The cells also display a perfect left/right symmetry about the position of permeability maximum. On the other hand, the cells due to the second mode for  $\nu = 0$  are perfectly out of phase with the mode 1 cells, and do not have this left/right symmetry.

When  $\nu = 1$ , the overall pattern now has period equal to four, again with strong cells appearing whenever the permeability is at its largest. In this case, the fluid motion within each neighbouring pair of strong cells is in the opposite direction, unlike for  $\nu = 0$ . The situation is more extreme when  $\nu = 0.5$  as strongly circulating cells occur at every other permeability maximum, and now the periodicity of the overall pattern is 8. It is highly unlikely that patterns for nonzero values of  $\nu$  are stable when entering the nonlinear regime, especially as they have a higher critical value of Ra. However, if  $P$  takes values other than 2, then patterns at nonzero values of  $\nu$  do become significant and will often form the primary mode of instability.

The values of  $\nu$  considered in Fig. 1 are a simple set of values, and some care must be taken when interpreting what different values of  $\nu$  mean when considering the overall periodicity of the pattern. When  $\nu$  takes rational fractional numbers such as  $m/n$ , where the fraction

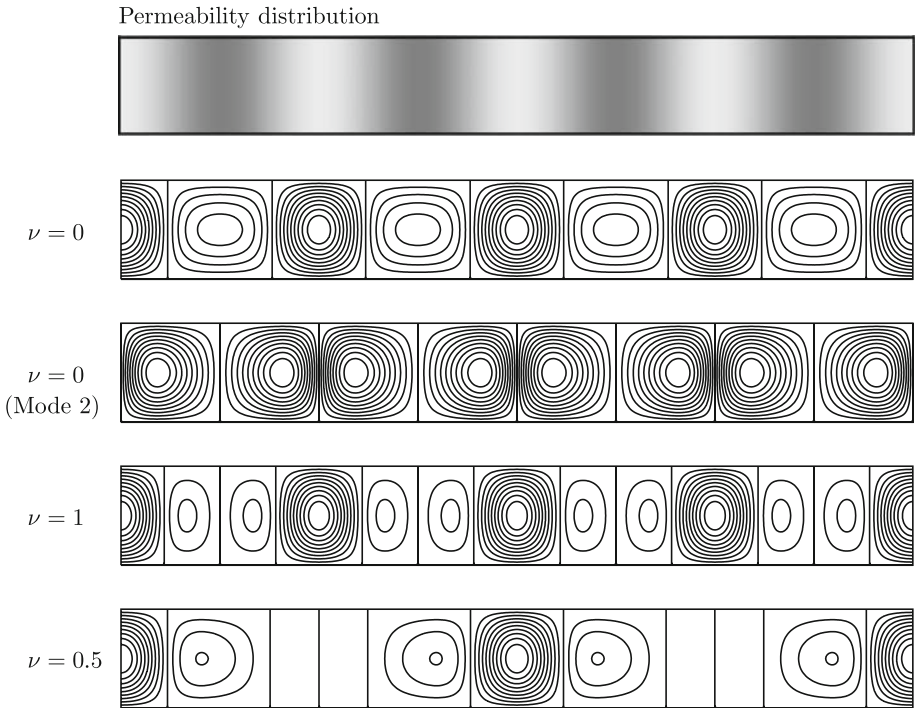


**Fig. 1** Streamlines corresponding to different onset modes with  $P=2$  and  $\epsilon=0.3$ . The grayscale frame shows the permeability distribution with lighter shades indicating higher permeability

lies between 0 and 1 and where  $m$  and  $n$  are relatively prime, then the overall pattern has periodicity equal to  $nP/m$  when  $m$  is even and  $n$  is odd and to  $2nP/m$  otherwise. When  $\nu$  is irrational the pattern is quasiperiodic.

Before leaving our consideration of Fig. 1 it is also worth noting that the isotherms for mode 1 for  $\nu=0$  are almost identical to the shape of the streamlines of mode 2, and vice versa, and therefore we have not presented these separately. Similarly, isotherms are always exactly out of phase with the streamline pattern and follow the same variations in amplitude.

Figure 2 shows how the streamlines change when the permeability amplitude,  $\epsilon$ , increases. At small values, such as  $\epsilon=0.1$ , there is little discernable difference between the cell centred at the permeability maximum and its neighbour at the minimum. However, as  $\epsilon$  increases the cell at the maximum grows in relative strength until values near  $\epsilon=0.9$ , the flow strength corresponding to the weaker cell achieves a magnitude which is  $<10\%$  of the that of the stronger cell. The pattern now appears to consist of a train of co-rotating cells with little fluid motion in between. Again, the depicted flow pattern for mode 2 when  $\epsilon=0.9$  is roughly the isotherm pattern corresponding to mode 1.

Figure 3 displays how a period-2 onset mode changes its appearance as the period of the permeability variations decreases. In this figure, we repeatedly halve the period from frame to frame in order to fit a whole number of periods of the permeability variation into a whole convection period. We have also attempted to depict the different permeability variations within each frame to aid the understanding of how the pattern changes as  $P$  changes.

We also note that the requirement of a having period-2 onset mode means that  $\nu$  needs to change as  $P$  changes. Having taken the value  $\epsilon=0.8$ , this means that there is a very strong

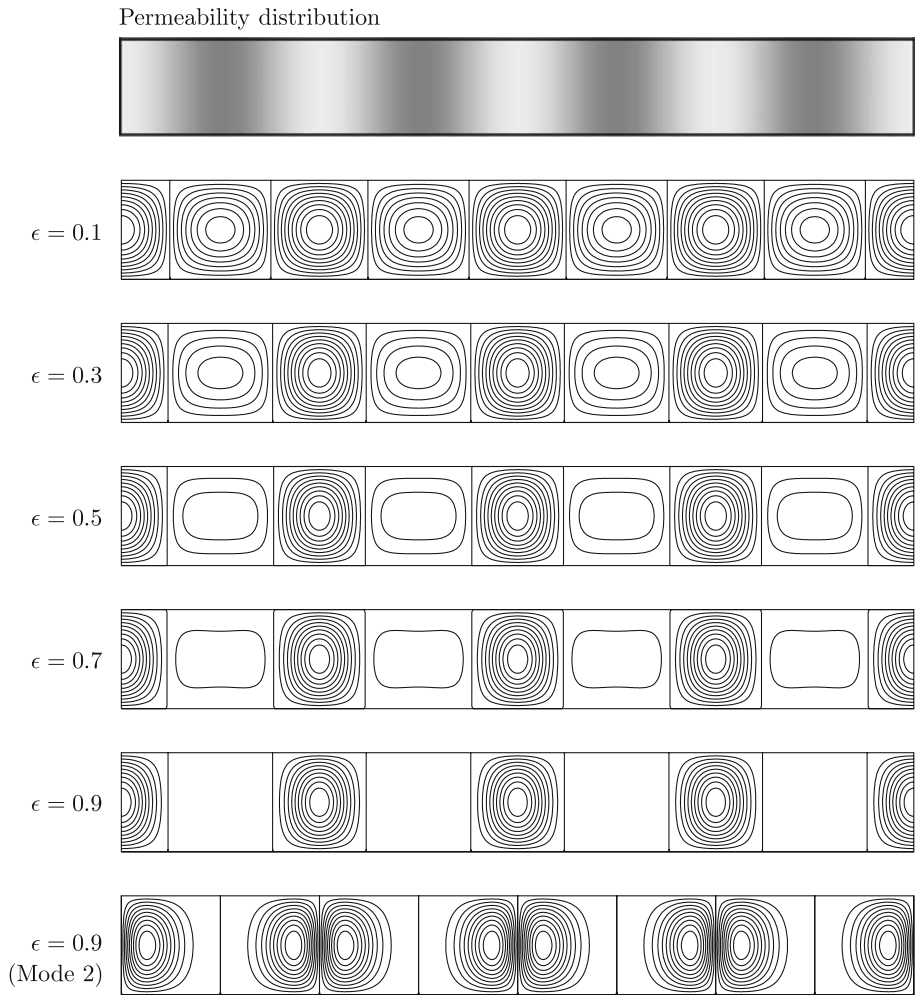


**Fig. 2** Streamlines corresponding to different permeability amplitudes,  $\epsilon$ , for  $P=2$  and  $\nu=0$ . Four periods are shown

change in permeability along the layer. Therefore when  $P=2$ , we see that the roll centred at the permeability maximum dominates with a very weak counter-circulation in-between. When  $P=1$  we have a counter-rotating train of identical roll shapes, each with left/right symmetry, and each cell is centred at the permeability maximum. Upon further reduction of the period to  $P=0.5$  and  $P=0.25$ , the patterns still retain this symmetry, but the streamlines now adopt a more complicated wavy pattern. It appears that there is a tendency for the flow to pass horizontally through the regions of high permeability in order to minimise the length of the path through these regions. Upon emergence into a high permeability region, the vertical velocity component increases quite markedly, and relatively rapid vertical jets of fluid are found there; this is seen most clearly for the  $P=0.25$  case.

Figure 4 shows how the primary onset mode changes as  $\epsilon$  increases when a large period,  $P=10$ , is taken and  $\nu$  has been set to zero. We now see that the permeability variation now

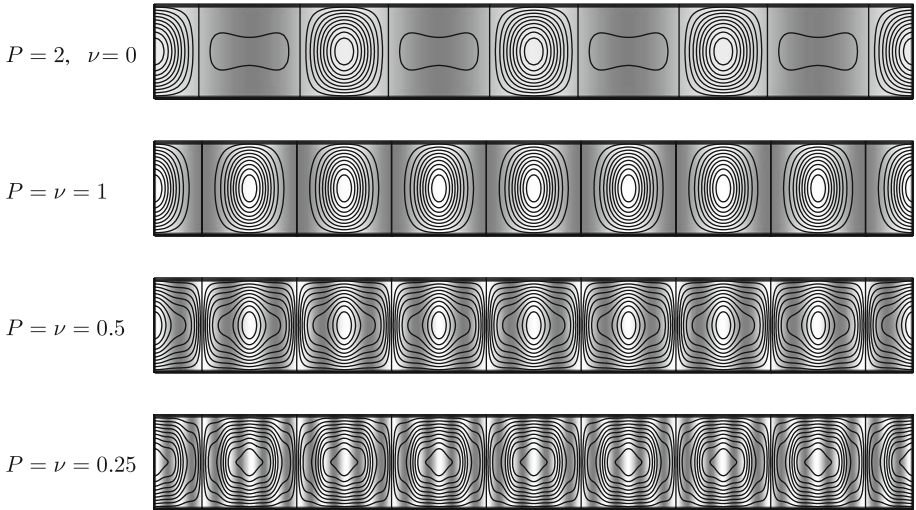


**Fig. 3** Streamlines corresponding to different onset modes with  $\epsilon = 0.8$ . The selected values of  $\nu$  yield patterns with periodicity equal to 2

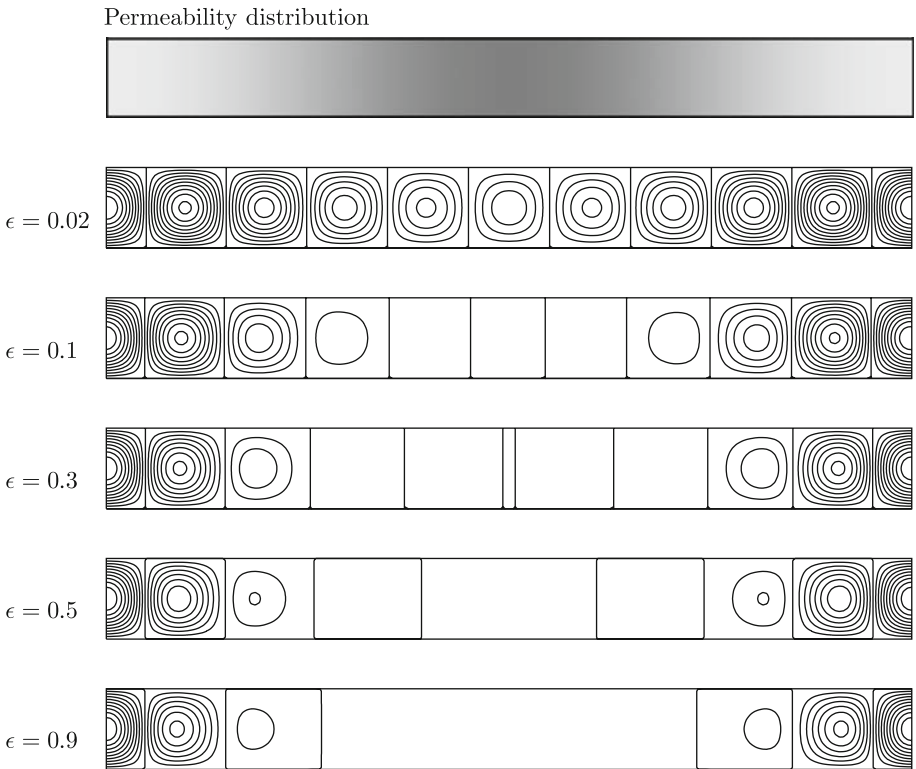


**Fig. 4** Streamlines corresponding to different onset modes with  $P = 10$  and  $\nu = 0$ . The greyscale frame shows the permeability distribution with lighter shades indicating higher permeability

has a strong effect even when  $\epsilon$  takes values as low as 0.02. Thus, there is a very clear reduction in the strength of the flow near to the permeability minimum compared with that at the maximum. Therefore, it is no surprise to see that convection soon becomes very localised as  $\epsilon$  increases, and more than half of the length of the cavity is in a near-quiescent state when  $\epsilon = 0.3$ . In fact, once the period of the permeability variation is sufficiently large (i.e. that the corresponding wavenumber,  $k$ , is sufficiently small) it is possible to show that the onset pattern is confined to a region of length of  $O(k^{-1/2})$ —see Appendix B—and that this is true for all nonzero values of  $\epsilon$ .

### 4.2 Neutral Curves

Having seen how the mode shapes vary with changes in the governing parameters, it now necessary to undertake a comprehensive set of computations to determine how the neutral curves themselves evolve with changes in the same parameters. Eight different values of  $P$  have been chosen as representative of this evolution. Figures 5 and 6 show the neutral curves for the first few modes for each of these periods and Ra is given as a function of  $\nu$  for the amplitudes  $\epsilon = 0, 0.2, 0.4$  and  $0.6$ . We note that these diagrams cover a whole period of  $\nu$ ;

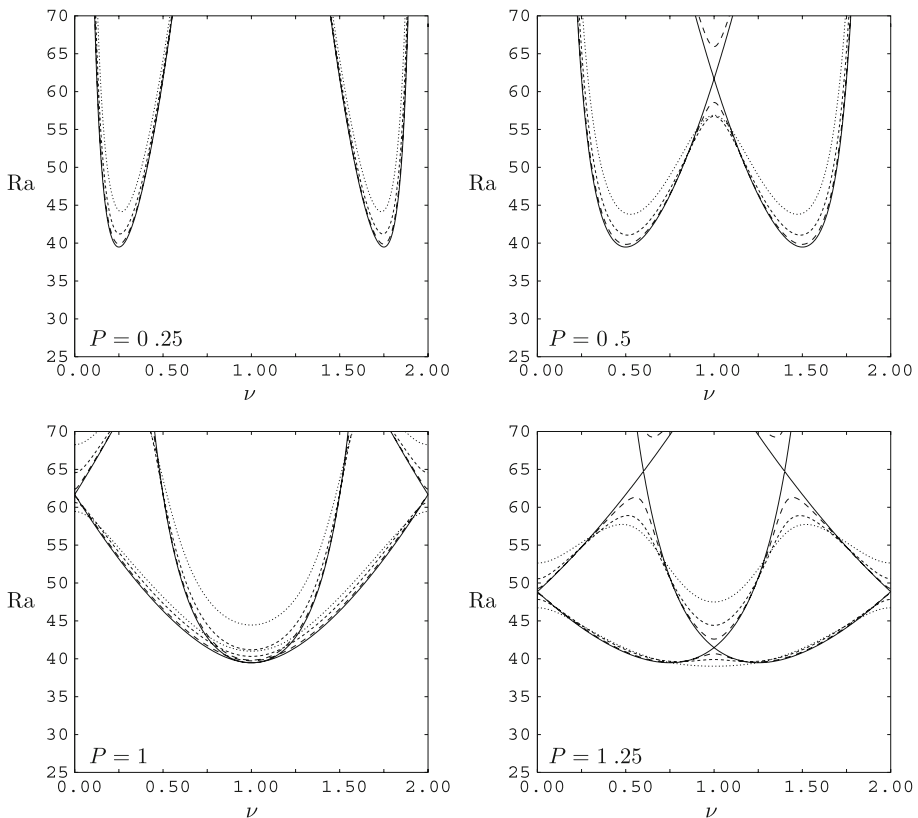


**Fig. 5** Neutral curves showing the variation of Ra with  $\nu$  for  $\epsilon = 0$  (continuous line), 0.2 (long dashes), 0.4 (short dashes), and 0.6 (dotted line). The different frames correspond to the shown values of  $P$ , the period of the permeability variation

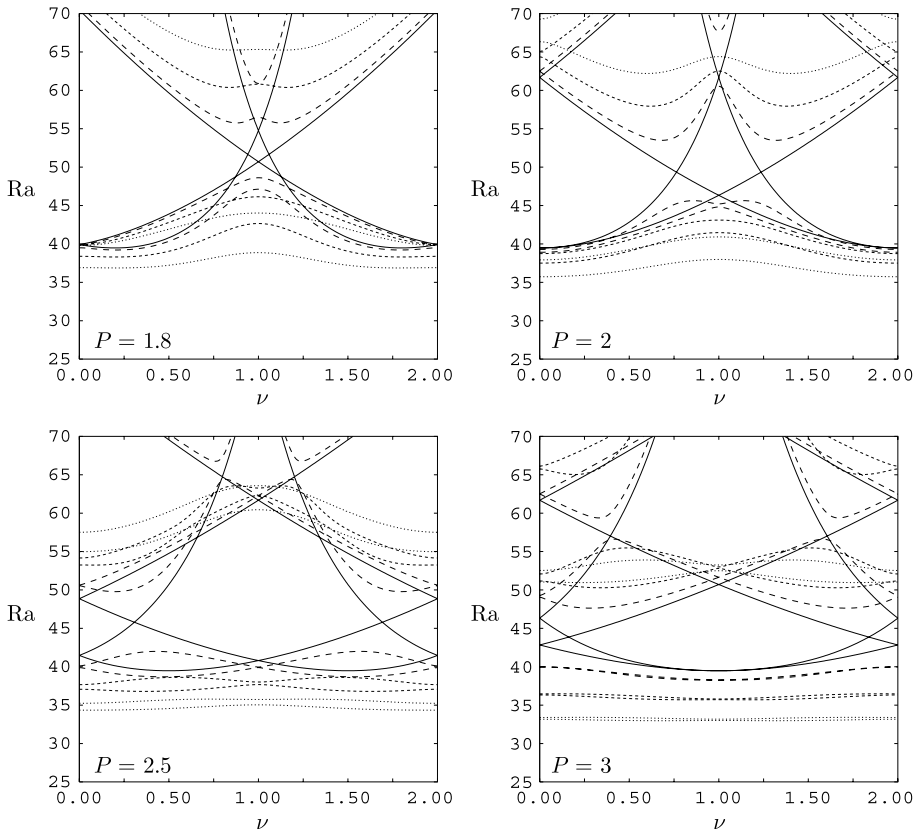


**Fig. 6** Neutral curves showing the variation of Ra with  $\nu$  for  $\epsilon = 0$  (continuous line), 0.2 (long dashes), 0.4 (short dashes), and 0.6 (dotted line). The different frames correspond to the shown values of  $P$ , the period of the permeability variation

further increases in  $\nu$  serve only to reproduce the same diagram, although individual curves do not have the same periodicity.

When  $P$  takes small values such as 0.25 and 0.5 a cursory glance at Fig. 5 suggests that the smallest value of Ra occurs when  $\nu = P$  (or, equivalently,  $\nu = 2 - P$ , which corresponds to the same convection pattern, i.e. those shown in Fig. 3). However, a closer inspection shows that the critical value of Ra corresponds to slowly increasing values of  $\nu$  as  $\epsilon$  increases. However, when the period becomes equal to unity, then all the amplitudes have their lowest critical value of Ra at  $\nu = 1$ , and the overall convection pattern looks like that shown in Fig. 3 for  $P = 1$ .

As  $P$  rises further, the critical value of  $\nu$  decreases again back towards zero, although the critical value for  $\epsilon = 0.6$  remains fixed at  $\nu = 1$  when  $P$  has increased to 1.25, suggesting that the amplitude of the permeability variation has a strong effect on the pattern of the primary mode of convection.

At still larger values of  $P$ , as shown in Fig. 6, this back-and-forth transition process, wherein the critical value of  $\nu$  varies between zero and unity, appears to continue. At these larger values of  $P$  we also see a further large- $\epsilon$  effect beginning to appear. Firstly, the critical value of Ra now decreases quite substantially from  $4\pi^2$ —this is in accord numerically with

the large- $P$  analysis contained in Appendix B. Secondly, there is a decreasing difference between the critical values of  $Ra$  for the first two modes. In addition, the  $\nu$ -dependence is also decreasing markedly. Here, the large- $P$  effect is such that convection cells appear in regions close to the permeability maxima with almost no flow in between these regions, as displayed in Fig. 4. Given the form of the convective amplitude function,  $A(\chi)$ , which is derived in Appendix B, and which exhibits super-exponential decay, it is very evident that the convection cells which arise near one permeability maximum are hardly coupled at all to those at neighbouring maxima. Thus, any  $\nu$ -dependence must be weak. Further, the analysis of Appendix B may be repeated for any phase of the basic roll state with no change in the value of the critical value of  $Ra$ , which explains why the neutral curves for large values of  $\epsilon$  when  $P = 3$  (and, more generally, for all non-zero values of  $\epsilon$  when  $P$  is large) are essentially independent of  $\nu$ .

### 4.3 Critical Curves: The Summary

Finally we are in a position to find the absolute minimum values of  $Ra$  for a suitably wide range of values of  $P$  and  $\epsilon$  by minimisation over  $\nu$ . Given how the minimising value of  $\nu$  varies, this has had to be done by a brute-strength numerical approach over a three-dimensional array of values of  $P$ ,  $\epsilon$  and  $\nu$ . The results of this process are shown in Figs. 7 and 8 where the former displays the critical Darcy–Rayleigh number, now denoted by  $Ra_c$ , and the latter the corresponding Floquet exponent,  $\nu_c$ .

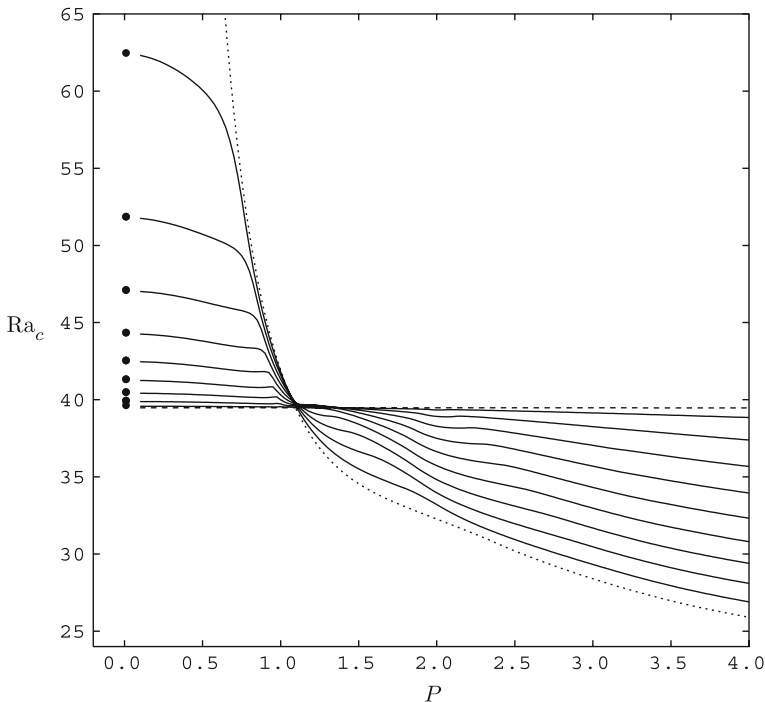


**Fig. 7** The variation of the critical value of  $Ra$  with  $P$ , the period of the permeability variation. The dashed line corresponds to  $\epsilon = 0$ , for which  $Ra_c = 4\pi^2$ . The dotted line corresponds to  $\epsilon = 0.994$ . Continuous lines correspond to  $\epsilon = 0.1, 0.2, \dots, 0.9$

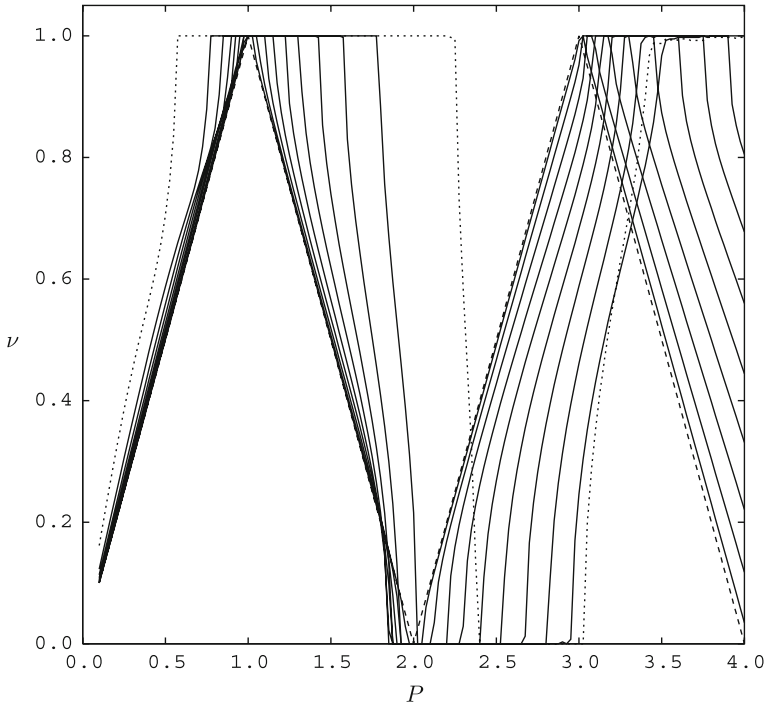


**Fig. 8** The variation with  $P$  of the value of  $\nu$  corresponding to the critical values of Ra shown in Fig. 7. The dashed line corresponds to  $\epsilon = 0$ , the dotted line to  $\epsilon = 0.99$ , while continuous lines correspond to  $\epsilon = 0.1, 0.2, \dots 0.9$

With regard to the critical value of Ra, the value  $P \simeq 1.1$  marks the transition between distinctively short period behaviour and distinctively large period behaviour and we discuss these limits in turn.

When  $P < 1$  convection cells pass through at least one, if not many, region of high permeability and therefore the porous medium may be regarded as being equivalent to an anisotropic homogeneous medium. The anisotropy is such that it causes the critical Darcy–Rayleigh number to rise above the classical value of  $4\pi^2$ . The easiest way to understand physically the effective anisotropy is by taking an analogy with electric conductors in parallel coupling (vertical) and series coupling (horizontal). The principle of parallel coupling implies that the effective permeability in the vertical  $z$ -direction is the average permeability  $K_0$ . The principle of series coupling implies that the effective permeability in the  $x$ -direction is  $K_0\sqrt{1 - \epsilon^2}$ . Physically this means that the average has been taken of the inverse permeability. If we extend the description of homogeneous anisotropy to the  $y$ -direction, the average permeability in that direction will also be  $K_0$ . Thus the average permeability in the  $y$ -direction is the same as the average permeability in the  $z$ -direction.

The anisotropic limit for the onset of two-dimensional convection in the  $(x, z)$ -plane is given by the critical Darcy–Rayleigh number

$$\text{Ra} = \pi^2(\xi^{-1/2} + 1)^2, \tag{23}$$

where the effective anisotropy parameter,  $\xi$ , is defined by

$$\xi = \sqrt{1 - \epsilon^2}. \tag{24}$$

This model of homogeneous anisotropy is asymptotically valid for small values of  $P$ . These results were derived by [Castinel and Combarnous \(1974\)](#), but also see [Kvernfold and Tyvand \(1979\)](#).

This anisotropic limit is valid asymptotically as  $P \rightarrow 0$ , and is included in [Fig. 7](#) as dots along the axis. These limiting values are in full agreement with our numerical results. Moreover, we observe graphically that the deviation from the anisotropic limit for  $P \ll 1$  is proportional to the square of  $P$ . The same result was found by [Gjerde and Tyvand \(1984\)](#) for the similar problem with continuous periodically stratified horizontal layers. This squared type of deviation is justified mathematically by observing that the onset problem is mathematically unchanged if we change the sign of  $P$ .

At the ‘transition’ point,  $P \simeq 1.1$ , the critical value of  $Ra$  is almost independent of  $\epsilon$ . However, when  $P > 1$  the convective process begins to be dominated by conditions near the permeability maxima. Given that  $Ra$  is based upon the mean permeability, this means that the critical values fall below  $4\pi^2$ . The manner in which this happens has been presented in [Appendix B](#).

When  $P$  lies in the range  $1.1 < P < 2.5$  the critical curves for  $Ra$  exhibit a wavy behaviour which may be traced to a very strong change in the corresponding value of the Floquet exponent shown in [Fig. 8](#). In this figure, we see that  $\nu_c$  is piecewise continuous when  $\epsilon = 0$ ; this is due to the fact that the Floquet exponent must take such values to maintain a convective wavelength of 2. As  $\epsilon$  rises the transition of  $\nu_c$  from zero to unity becomes faster and the range of values of  $P$  over which  $\nu_c$  takes the values 0 or 1 increases in size. For example, when  $\epsilon = 0.99$ ,  $\nu_c = 1$  for the whole of the range  $0.6 < P < 2.25$ .

At still larger values of  $P$  (not shown), the critical values of  $Ra$  decay in the manner detailed in [Appendix B](#). However, the critical values of  $\nu$  become increasingly difficult to obtain due to decreasing variation of the neutral curves with changes in  $\nu$ . In fact, the detailed values of  $\nu$  become increasingly irrelevant as  $P$  increases due to the localisation of the convection pattern.

## 5 Discussion

In this article, we have used a Floquet analysis to determine the primary modes of instability for convection in a horizontal porous layer with horizontal periodic variations in the permeability. The governing equations were solved numerically using a highly accurate matrix eigenvalue method and these results supplemented by a multi-scales analysis when the period of the permeability variations is large. Some detailed flow patterns were given, which allowed for a detailed physical explanation of the large and small- $P$  behaviour of the system as a whole.

It is now quite natural to ask whether three-dimensional effects are likely to be more important. It is certainly well known that one-dimensional imperfections of the classical Darcy–Bénard problem often yield a three-dimensional flow field at onset. The articles by [Rees and Riley \(1986, 1989a\)](#), which consider resonant and nearly resonant boundary imperfections, respectively, find that longitudinal rolls are often favoured, and in this context, we would expect cells of unit aspect ratio to form the primary mode since the layer is isotropic in the  $y$ -,  $z$ -plane. However, [Rees and Riley \(1989a\)](#) also found that wavy rolls are sometimes obtained and which are initiated by the action of the zigzag instability. On the other hand, when the boundary imperfections take non-resonant wavenumbers then quite a variety of patterns may form the primary mode, including rectangular cells (see [Rees and Riley \(1989b\)](#)). It is quite likely that the present configuration may retain some of the qualitative features

of these articles. However, as previously mentioned, these results apply for layers that are sufficiently confined in the  $y$ -direction, or for experimental models using the Hele–Shaw cell.

This article has not considered the effect of periodic variations in the thermal diffusivity of the porous layer. The presence of such variations would not affect the basic state, which would again consist of a linear temperature profile and no flow. As regard two-dimensional convection, we doubt that it would cause any new qualitative effects to those presented here. On the other hand, if we were to relax the insistence that permeability and diffusivity variations are in one direction, such as in the blocked configuration considered by [Nield et al. \(2009\)](#), then the basic state consists of a more complicated temperature field and a non-zero basic flow. In an horizontally unbounded but periodic domain, a similar Floquet analysis could be undertaken, but the equations that would replace Eqs. 21 and 22 would be two-dimensional for two-dimensional convection and three-dimensional for three-dimensional convection. Such analyses are tractable, but would take much longer to complete than those presented here.

**Acknowledgements** The authors would like to thank the reviewers for their perceptive comments.

### Appendix A: The Numerical Method

Equations 21 and 22 were discretised using various central difference formulae. The code was written with an option to use either second, fourth, sixth or eighth order formulae. We will use the notation,  $f_i$ , to denote the numerical approximation to  $f(x)$  at  $x_i$ , i.e. at the  $i^{\text{th}}$  grid point of a uniform grid. If we define the coefficients,  $a_j$  and  $b_j$ , as the coefficients for the finite difference approximations,

$$f'(x_i) \sim h^{-1} \sum_j a_j f_{i+j}, \quad f''(x_i) \sim h^{-2} \sum_j b_j f_{i+j}, \tag{25}$$

where  $h$  is the uniform steplength, then these coefficients are given by the entries in Tables 1 and 2 below.

**Table 1** Coefficients of the central difference approximations to  $f'$ . Note that  $a_{-j} = -a_j$

Order	$a_0$	$a_1$	$a_2$	$a_3$	$a_4$
Second	0	$\frac{1}{2}$	0	0	0
Fourth	0	$\frac{2}{3}$	$-\frac{1}{12}$	0	0
Sixth	0	$\frac{3}{4}$	$-\frac{3}{20}$	$\frac{1}{60}$	0
Eighth	0	$\frac{4}{5}$	$-\frac{1}{5}$	$\frac{4}{105}$	$-\frac{1}{280}$

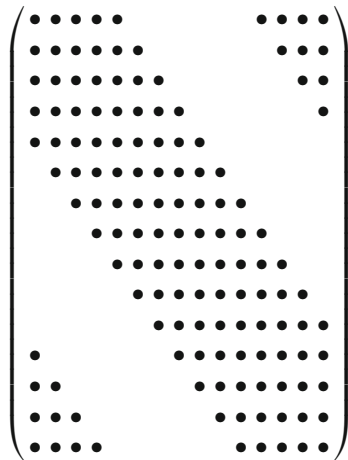
**Table 2** Coefficients of the central difference approximations to  $f''$ . Note that  $b_{-j} = b_j$

Order	$b_0$	$b_1$	$b_2$	$b_3$	$b_4$
Second	-2	1	0	0	0
Fourth	$-\frac{5}{2}$	$\frac{4}{3}$	$-\frac{1}{12}$	0	0
Sixth	$-\frac{49}{18}$	$\frac{3}{2}$	$-\frac{3}{20}$	$\frac{1}{90}$	0
Eighth	$-\frac{205}{72}$	$\frac{8}{5}$	$-\frac{1}{5}$	$\frac{8}{315}$	$-\frac{1}{560}$

If we also define  $\underline{f}$  and  $\underline{g}$  to be the vectors of the unknown values of  $f_i$  and  $g_i$ , respectively, then Eqs. 21 and 22 may be written in the matrix/vector forms,

$$M_1 \underline{f} = Ra M_2 \underline{g}, \quad M_3 \underline{f} = M_4 \underline{g}, \tag{26}$$

where  $M_k, k = 1,4$ , are complex matrices of dimension  $N \times N$  when  $N$  intervals are used in the range,  $0 \leq x \leq P$ . For the eighth order method, these matrices have the periodic banded structure,



$$\tag{27}$$

and we note that the band is narrower for the lower order methods. The vector  $\underline{g}$  may now be eliminated from Eq. 26 to yield the following generalised eigenvalue problem for Ra,

$$M_1 \underline{f} = Ra [M_2 M_4^{-1} M_3] \underline{f}. \tag{28}$$

Equation 28 was solved using the NAG library routine F02GJF which employs the QZ algorithm to obtain the eigenvalues and their corresponding eigenvectors. The lowest value of Ra forms the primary mode of instability for given values of  $P$  and  $\nu$ .

The absolute accuracy of the computed values of Ra is of paramount importance and forms the main reason why we have used an eighth order method. Table 3 contains the computed values of Ra corresponding to the primary mode for the case,  $P = 2$  and  $\nu = 0.3$ , together with the relative accuracy of the same data in Table 3.

As may be seen in Table 3, the error in the computed data decreases at a rate which is appropriate for the order of accuracy of the discretisation. So for the second order scheme the

**Table 3** Critical values of Ra for  $P = 2$  and  $\nu = 0.3$

Order:	Values of Ra				Values of Ra/Ra <sub>exact</sub>			
	Second	Fourth	Sixth	Eighth	Second	Fourth	Sixth	Eighth
10	41.453028	37.952028	37.344271	37.172816	1.118601	1.024127	1.007727	1.003100
20	38.369158	37.134304	37.064836	37.058752	1.035384	1.002061	1.000187	1.000023
40	37.409174	37.062969	37.058043	37.057929	1.009479	1.000136	1.000003	1
80	37.147232	37.058243	37.057927	37.057925	1.002410	1.000009	1	1
160	37.080344	37.057940	37.057920	37.057920	1.000605	1.000001	1	1

errors decrease by a factor of roughly  $2^2$  when  $N$  doubles, and by factors of  $2^4$  and  $2^6$  for the fourth and sixth order methods, and so on. It is clear that the accuracy of the eighth order method can exceed 6 significant figures even for as few as  $N = 40$  intervals. As the accuracy of higher modes tends to decrease as the mode number increases, we have generally adopted 100 intervals for our calculations.

### Appendix B: The Large- $P$ Analysis

In this Appendix, we outline the large- $P$  (equivalently, small- $k$ ) analysis of the onset of convection. For simplicity, we shall set  $v = 0$  (equivalently,  $\omega = 0$ ). Subject to this, Eqs. 21 and 22 reduce to the form,

$$f'' - \pi^2 f + \frac{k\epsilon \sin kx}{1 + \epsilon \cos kx} f' = \text{Ra} (1 + \epsilon \cos kx) g', \tag{29}$$

$$g'' - \pi^2 g + f' = 0, \tag{30}$$

Recall that  $F(x) = 1 + \epsilon \cos(kx)$ , where  $k$  is now taken to be small, but  $\epsilon$  remains of  $O(1)$  in magnitude. The numerical evidence of Fig. 4 suggests that cells only occupy a region close to where the permeability takes its maximum value, and therefore we shall concentrate on the region near  $x = 0$ . It will be necessary to adopt a multiple-scales approach similar to that of Rees (1990) to determine the onset of convection since we expect cells to have an  $O(1)$  wavelength, but the onset pattern extends over many cells. It turns out that the appropriate lengthscale to use is one which is of  $O(k^{-1/2})$ , which is asymptotically large compared with that of the cell wavelength, but asymptotically small compared with  $O(k^{-1})$ , the wavelength of the permeability variations. Therefore we define the slow spatial scale,  $\chi$ , according to,

$$\chi = k^{1/2}x, \tag{31}$$

and expand the solutions of Eqs. 21b and 30 in powers of  $k^{1/2}$ :

$$(f, g, \text{Ra}) = \sum_{i=0} k^{i/2} (f_i(x, \chi), g_i(x, \chi), R_i), \tag{32}$$

where the summation is over positive integers. Given the presence of two spatial scales, this means that the second  $x$ -derivative must be modified and replaced, as follows:

$$\frac{d^2}{dx^2} \longrightarrow \frac{\partial^2}{\partial x^2} + 2 \frac{\partial^2}{\partial x \partial \chi} + \frac{\partial^2}{\partial \chi^2}. \tag{33}$$

At leading order, we obtain the system,

$$f_0'' - \pi^2 f_0 - R_0(1 + \epsilon)g_0' = 0, \tag{34}$$

$$g_0'' - \pi^2 g_0 + f_0' = 0. \tag{35}$$

This system is almost exactly the one which corresponds to the classical Darcy–Bénard problem. The solution is,

$$f_0 = 2\pi A(\chi) \sin \pi x, \quad g_0 = A(\chi) \cos \pi x, \quad R_0 = \frac{4\pi^2}{1 + \epsilon}, \tag{36}$$

where  $A(\chi)$  is a slowly varying amplitude of the convective wave packet. At  $O(k^{1/2})$  the equations are

$$f_1'' - \pi^2 f_1 - R_0(1 + \epsilon)g_1' = R_1(1 + \epsilon)g_0', \tag{37}$$

$$g_1'' - \pi^2 g_1 + f_1' = 0. \tag{38}$$

It is essential to set  $R_1 = 0$  otherwise these equations cannot be solved. Although this leaves the same autonomous system as the leading order system, we set  $f_1 = g_1 = 0$ , as it is always possible to adjust the definition of the solution for  $f_0$  and  $g_0$  to yield zero solutions for  $f_1$  and  $g_1$ .

At  $O(k)$  we obtain,

$$f_2'' - \pi^2 f_2 - R_0(1 + \epsilon)g_2' = R_2(1 + \epsilon)g_0' - \frac{1}{2}R_0\epsilon\chi^2g_0' - f_{0,\chi\chi}, \tag{39}$$

$$g_2'' - \pi^2 g_2 + f_2' = -g_{0,\chi\chi}, \tag{40}$$

where the  $\chi$ -subscripts indicate partial derivatives with respect to  $\chi$ . A simple solvability condition may be applied in order obtain an equation relating  $A(\chi)$  and  $R_2$ ; we find that

$$\frac{1}{4}R_2(1 + \epsilon)A - \frac{1}{8}\epsilon R_0\chi^2A + A_{\chi\chi} = 0. \tag{41}$$

This equation has the form of a parabolic cylinder function, and the simple scaling,

$$\chi = \left(\frac{32}{\epsilon R_0}\right)^{1/4} \hat{\chi}, \tag{42}$$

reduces it to the form,

$$\left(\frac{2}{\epsilon R_0}\right)^{1/2} R_2(1 + \epsilon)A - 4\hat{\chi}^2A + A_{\hat{\chi}\hat{\chi}} = 0. \tag{43}$$

The simplest solution of this equations (and indeed its first mode) is given by  $A = \exp(-\hat{\chi}^2)$ , provided that the leading coefficient in Eq. 43 is precisely two. Therefore we eventually obtain,

$$R_2 = \frac{(2\epsilon R_0)^{1/2}}{1 + \epsilon} = \frac{2\pi\sqrt{2\epsilon}}{(1 + \epsilon)^{3/2}}. \tag{44}$$

We may now state that the critical value of Ra in the large- $P$  or small- $k$  limit is,

$$Ra_c \sim \frac{4\pi^2}{1 + \epsilon} + \frac{2\pi\sqrt{2\epsilon}}{(1 + \epsilon)^{3/2}}k. \tag{45}$$

The following Table gives some comparisons between our computed values of  $Ra_c$  and those given by Eq. 45. Table 4

**Table 4** comparison between the numerical and the asymptotic solutions for  $Ra_c$  when  $P = 10$  (i.e.  $k = \pi/5$ )

$\epsilon$	$Ra_c$ (Num)	$Ra_c$ (Asymp)
0.1	36.6502	36.6546
0.5	27.4244	27.3934
0.9	21.8288	21.7893

## References

- Beck, J.L.: Convection in a box of porous material saturated with fluid. *Phys. Fluids* **15**, 1377–1383 (1972)
- Castinel, G., Combarous, M.: Critère d'apparition de la convection naturelle dans une couche poreuse anisotrope horizontale. *C. R. Acad. Sci.* **B278**, 701–704 (1974)
- Ephere, J.F.: Critère d'apparition de la convection naturelle dans une couche poreuse anisotrope. *Rev. Gen. Thermique.* **168**, 949–950 (1975)
- Gheorghitza, S.I.: The marginal stability in porous inhomogeneous media. *Proc. Camb. Phil. Soc.* **57**, 871–877 (1961)
- Gjerde, K.M., Tyvand, P.A.: Thermal convection in a porous medium with continuous periodic stratification. *Int. J. Heat Mass Transf.* **27**, 2289–2295 (1984)
- Horton, C.W., Rogers, F.T.: Convection currents in a porous medium. *J. Appl. Phys.* **16**, 367–370 (1945)
- Kvernfold, O., Tyvand, P.A.: Nonlinear thermal convection in anisotropic porous media. *J. Fluid Mech.* **90**, 609–624 (1979)
- Lapwood, E.R.: Convection of a fluid in a porous medium. *Proc. Camb. Phil. Soc.* **44**, 508–521 (1948)
- McKibbin, R.: Heat transfer in a vertically layered porous medium heated from below. *Transp. Porous Med.* **1**, 361–370 (1986)
- McKibbin, R., O'Sullivan, M.J.: Onset of convection in a layered porous medium heated from below. *J. Fluid Mech.* **96**, 375–393 (1980)
- McKibbin, R., O'Sullivan, M.J.: Heat transfer in a layered porous medium heated from below. *J. Fluid Mech.* **111**, 141–173 (1981)
- McKibbin, R., Tyvand, P.A.: Anisotropic modelling of thermal convection in multilayered porous media. *J. Fluid Mech.* **18**, 315–319 (1982)
- McKibbin, R., Tyvand, P.A.: Thermal convection in a porous medium composed of alternating thick and thin layers. *Int. J. Heat Mass Transf.* **26**, 761–780 (1983)
- McKibbin, R., Tyvand, P.A.: Thermal convection in a porous medium with horizontal cracks. *Int. J. Heat Mass Transf.* **27**, 1007–1023 (1984)
- Nield, D.A., Bejan, A.: *Convection in Porous Media* (3rd edn). Springer, New York (2006)
- Nield, D.A., Kuznetsov, A.V., Simmons, C.T.: The effect of strong heterogeneity on the onset of convection in a porous medium: non-periodic global variation. *Transp. Porous Med.* doi:[10.1007/s11242-008-9297-6](https://doi.org/10.1007/s11242-008-9297-6) (2009)
- Poulikakos, D., Bejan, A.: Natural convection in vertically and horizontally layered porous media heated from the side. *Int. J. Heat Mass Transf.* **26**, 1805–1814 (1983)
- Rana, R., Horne, R.N., Cheng, P.: Natural-convection in a multi-layered geothermal reservoir. *ASME J. Heat Transf.* **101**, 411–416 (1979)
- Reda, D.C.: Natural-convection experiments in a stratified liquid-saturated porous medium. *ASME J. Heat Transf.* **108**, 660–666 (1986)
- Rees, D.A.S.: The effect of long-wavelength thermal modulations on the onset of convection in an infinite porous layer heated from below. *Quart. J. Mech. Appl. Math.* **43**, 189–214 (1990)
- Rees, D.A.S.: The stability of Darcy–Bénard convection. In: Vafai, K. (ed.) *Handbook of Porous Media*, pp. 521–558. Marcel Dekker (2000)
- Rees, D.A.S., Lage, J.L.: The effect of thermal stratification on natural convection in a vertical porous insulation layer. *Int. J. Heat Mass Transf.* **40**, 111–121 (1997)
- Rees, D.A.S., Riley, D.S.: Convection in a porous layer with spatially periodic boundary conditions: resonant wavelength excitation. *J. Fluid Mech.* **166**, 503–530 (1986)
- Rees, D.A.S., Riley, D.S.: The effects of boundary imperfections on convection in a saturated porous layer: near-resonant wavelength excitation. *J. Fluid Mech.* **199**, 133–154 (1989a)
- Rees, D.A.S., Riley, D.S.: The effects of boundary imperfections on convection in a saturated porous layer: non-resonant wavelength excitation. *Proc. R. Soc. Lond.* **A421**, 303–339 (1989b)
- Rees, D.A.S., Riley, D.S.: The three-dimensional stability of finite-amplitude convection in a layered porous medium heated from below. *J. Fluid Mech.* **211**, 437–461 (1990)
- Rees, D.A.S., Tyvand, P.A.: The Helmholtz equation for convection in two-dimensional porous cavities with conducting boundaries. *J. Eng. Math.* **49**, 181–193 (2004a)
- Rees, D.A.S., Tyvand, P.A.: Oscillatory convection in a two-dimensional porous box with asymmetric lateral boundary conditions. *Phys. Fluids.* **16**, 3706–3714 (2004b)
- Wooding, R.A.: Steady state free thermal convection of liquid in a saturated permeable medium. *J. Fluid Mech.* **2**, 273–285 (1957)
- Wooding, R.A.: Large-scale geothermal field parameters and convection theory. *N. Z. J. Sci.* **21**, 219–228 (1978)